PHYSICAL REVIEW B VOLUME 50, NUMBER 15 15 OCTOBER 1994-I

Electromodulation spectroscopy of an array of modulation-doped GaAs/$Ga_{1-x}Al_xAs$ quantum dots: Experiment and theory

Godfrey Gumbs* and Danhong Huang†
Department of Physics and Astronomy, Hunter College of the City University of New York, 695 Park Avenue, New York, NY 10021

H. Qiang and Fred H. Pollak*
Department of Physics and New York State Center for Advanced Technology in Ultrafast Photonic Materials and Applications, Brooklyn College of the City University of New York, Brooklyn, New York 11210

P. D. Wang, C. M. Sotomayor Torres, and M. C. Holland
Nanoelectronics Research Center, Department of Electronics and Electrical Engineering, University of Glasgow, Glasgow G12 8QQ, Scotland
(Received 28 April 1994)

A recent photoreflectance (PR) experiment on a GaAs/$Ga_{1-x}Al_xAs$ modulation-doped quantum dot array shows that at 77 K the quasi-two-dimensional "2C-2H" interband transition develops a series of evenly spaced oscillations. Such features are due to the quantization of the energy levels related to the in-plane paraboliclike potential for such reduced-dimensional systems, e.g., evenly spaced conduction and valence subbands. However, for the other dominant feature, i.e., "1C-1H"/"1C-1L," no fine structure is observed since the first electron subband is occupied. We present a self-consistent field theory and numerical calculations for the intersubband absorption coefficient of an array of GaAs/$Ga_{1-x}Al_xAs$ quantum dots with lateral parabolic confining potentials for electrons and holes. Our numerical results for the derivative of the absorption coefficient have features which are quite similar to those observed in the PR experiment.

I. INTRODUCTION

There has recently been considerable activity in the field of reduced-dimensional systems such as one-dimensional (1D) quantum wires (QW's) and zero dimensional (0D) quantum dots (QD's) from both fundamental and applied perspectives.[1–15] Considering the huge success of physics and devices based on two-dimensional (2D) semiconductor systems (i.e., quantum wells, superlattices, heterojunctions), there has been a natural trend to continue to reduce the dimensionality of these systems. These reduced-dimensional nanostructures exhibit interesting properties involving singularities in the density of states and unique transport phenomena.[1,2] For QD's, the ultimate goal is an artificial atom with a tunable number of electrons. In 0D systems, evidence has been found for a paraboliclike in-plane confining potential,[1] as opposed to the square well potential along the growth direction. Interesting transport phenomena such as Coulomb blockade have been demonstrated in quantum dots.[1,15,16] Optical applications include low-threshold, high-yield laser structures and photodetectors.[3–5]

One- and zero-dimensional systems can be formed in several ways. For example, 2D structures are easily obtained in the growth direction by thin film methods such as molecular beam epitaxy (MBE) or organometallic chemical vapor deposition. Therefore an obvious way to obtain QW and QD arrays is to pattern the usual 2D heterostructures such as QW's with nanoscale lithographic techniques.[17] More recently, quantum dots have been made by placing tiny gate electrodes on top of a buried layer that confines electrons in two dimensions. The voltage of these electrodes squeezes the electrons into regions of confinement. By varying this external gate voltage, the shape and size of a quantum dot and the number of electrons within the dot can be adjusted. Large periodic arrays of quantum dots have been fabricated using gridlike gate electrodes. When a voltage is applied to the grid, a regular lattice of dots is formed in the underlying material. The size, shape, and symmetry of the confining potential are determined by the shape of the gate electrodes. The strength of the confining potential regulates the number of electrons in each dot. However, the lack over control of the defects in the underlying quantum well material and the imperfections in the electrode grid makes it difficult to produce an array of identical dots.

Despite the proven value of modulation spectroscopy, particularly contactless modes such as photoreflectance (PR), in studying 2D systems,[18,19] there has been very little work done on either 1D or 0D nanostructures. In PR (a contactless form of electromodulation) modulation of the built-in electric field in the sample is caused by photoexcited electron-hole pairs created by a pump source (laser or other light source) which is chopped at frequency Ω_m. This procedure results in sharp derivativelike spectral features in the region of intersubband transitions. In reduced-dimensional systems, it has been

shown that PR produces a line shape which is the first derivative of the unmodulated optical constants.[18,19] Photoreflectance has been used to study 1D SiGe/Si quantum wires[20] and the effects of reactive ion etching on large ($\approx$ 0.5 μm) GaAs/$Ga_{1-x}Al_xAs$ QD arrays.[21] Several authors have measured the electrotransmission spectra of CdS_xSe_{1-x} nanocrystals embedded in a glass matrix.[22] A preliminary PR investigation of modulation-doped GaAs/$Ga_{0.73}Al_{0.27}As$ QD arrays (lateral dimensions of 60 nm and 100 nm) at 77 K and 300 K has been reported.[23] Even at room temperature, it was possible to detect the effects of the lateral quantum confinement, e.g., a 2 meV blueshift of the spectral feature $2C$-$2H$ of the smaller sized QD array in relation to the 100 nm QD sample. At 77 K this resonance in the 60 nm array exhibited a series of evenly spaced oscillations. This effect was interpreted in terms of the quantization of the energy levels related to the in-plane paraboliclike potential for such reduced-dimensional systems, e.g., evenly spaced conduction and valence subbands for a paraboliclike in-plane confining potential on the smaller QD array.

In this paper, we present a self-consistent field theory for the absorption coefficient of an array of modulation-doped GaAs/$Ga_xAl_{1-x}As$ QD's at arbitrary temperature. We simulate the confining potential due to the surface charge on the QD's by lateral parabolic confining potentials for the electrons and holes. When the derivative of the absorption coefficient is taken with respect to the photon energy, the details of the spectral features are greatly amplified. This model gives a quantitative way of determining the confining environment associated with the QD's. These calculations are compared with the recent PR experiment of Ref. 23. By using this theoretical approach, Gumbs, *et al.*[24] were able to accurately obtain a number of important parameters, i.e., the 2D electron gas density, quantum well width, alloy composition, built-in electric fields, and strain, in pseudomorphic $Ga_{1-x}Al_xAs/In_yGa_{1-y}As$/GaAs modulation-doped quantum wells (MDQW's) that form the basis for high electron mobility transistors. The numerical results of Ref. 24 compared well with the contactless electroreflectance (CER) data for the intersubband transitions of a pseudomorphic $Ga_{0.81}Al_{0.19}As/In_{0.20}Ga_{0.80}As$/GaAs MDQW over a wide temperature range (17 K$< T <$351 K). Furthermore, the low-intensity light used in this method reduces the possibility of any spurious effects on the evaluation of the electron density due to photoexcited carriers. The simple one-electron line shape fit to the spectrum is found to be reasonable only for the peaks observed at high temperature for which many-body effects are small.[25–27] The Fermi edge transitions at low temperatures cannot be modeled by the one-electron theory. The theory which we present in this paper for the interband absorption characterization of quantum dots includes the depolarization shift due to the electron-electron interaction, impurity scattering, and the effect due to interface imperfection.

The PR data at 77 K for the 60 nm dot array of Ref. 23 showed that a major spectral feature, i.e., the quasi-2D "$2C$-$2H$" transition, develops a number of evenly spaced secondary peaks associated with the discrete energy levels in the QD's. However, no such oscillations are observed for the other dominant feature, i.e., "$1C$-$1H$"/"$1C$-$1L$," since the first electron subband is occupied. The line shape of this resonance suggests a screened exciton associated with the electrons and holes in different subbands. In such a 0D system with cylindrical symmetry, the electron (hole) energy levels will be characterized by three quantum numbers, i.e., $n_zC[H(L)]$, $n_yC[H(L)]$ and $n_xC[H(L)]$. For example, $n_zC[H(L)]$ corresponds to the conduction (C) or heavy (H)/light (L) hole subbands along the growth (z) direction, while the other two quantum numbers specify the in-plane quantization. The notation m_zC-$n_zH(L)$ denotes a transition between the m_zth conduction and n_zth valence subbands of heavy (light) hole character. Rigorously speaking, the notation should include three quantum numbers for both the electrons and holes because of the effects of the lateral confinement. In this paper, we use "m_zC-$n_zH(L)$" to indicate the quasi-2D transitions.

The rest of this paper is organized as follows. In Sec. II, the experimental details and results are given. In Sec. III, we present an analytic result for the absorption coefficient in a quantum-dot array when a dynamic dipole in the system is induced by an external electric field. This formalism includes the polarization angle and temperature dependencies. Section IV contains numerical results for the absorption coefficient of unpolarized incident light and its frequency derivative for a square array of quantum dots. A summary of our results follows in Sec. V.

II. EXPERIMENTAL DETAILS AND RESULTS

The PR apparatus has been described in the literature.[18,19] The pump beam was the 6328 Å line of a He-Ne laser chopped at 200 Hz. The sample used in this study was grown by MBE on a (001) semi-insulating GaAs substrate with a 1 μm not-intentionally-doped GaAs buffer.[23] The active region was a 0.58 μm thick multiple quantum well (MQW) structure which consisted of the following layers repeated ten times: a 30 nm $Ga_{1-x}Al_xAs$ layer, a Si δ-doping layer (2×10^{12} cm^{-2}), 20 nm of a GaAs (0.85 nm)/AlAs (0.85 nm) superlattice structure, and an 8 nm GaAs QW region. There was a 17 nm GaAs cap on top of the entire structure. Shubnikov–de Haas measurements indicated that the electron gas (EG) density in the GaAs QW's corresponded to a "two-dimensional" concentration of 8.5×10^{11} cm^{-2}. Thus the Fermi energy is about 20 meV above the first conduction subband. The 60 nm QD arrays formed a square lattice pattern, with the separation between neighboring dots being four times the individual dot diameter. The lateral dimension of this QD array is sufficiently small to produce an observable lateral quantum confinement effect. In Ref. 23, a blueshift of $2C$-$2H$ of the 60 nm array in relation to a 100 nm array was observed at 300 K. The magnitude of the shift was consistent with the effects of the lateral confinement.

Displayed in Fig. 1 is the PR spectrum of the QD array at 77 K. The structure around 1.5 eV is from the

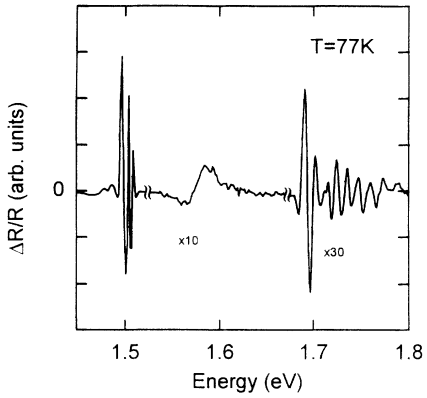

FIG. 1. Experimental photoreflectance spectrum at $T = 77$ K for a 60 nm quantum dot array as a function of the incident photon energy. The $2C$-$2H$ transition at about 1.7 eV from the second heavy-hole subband to the second electron subband develops a series of oscillations corresponding to the excitations between the discrete energy levels of lateral confinement.

direct gap E_0 of the GaAs buffer/substrate. The signal around 1.6 eV is quite unusual for modulation spectroscopy from a QW system. Such traces generally exhibit sharp, derivativelike features (i.e., positive and negative lobes) associated with excitons, even at 300 K. In addition, these reported line shapes are symmetric.[18,19] The 1.6 eV trace of Fig. 1 lies on only one side of the baseline and corresponds to the screened $1C$-$1H$/$1C$-$1L$ excitonic transitions. The screening is due to the presence of the EG. Yin *et al.*[25,27] and Dimoulas *et al.*[26] have recently observed similar signals in PR associated with the 2D EG in $Ga_{1-x}Al_xAs/In_yGa_{1-y}As/GaAs$ MDQW's. Such lineshapes were accounted for on the basis of the first-derivative of a broadened steplike 2D density of states (due to the screening of the exciton) times a Fermi level filling factor.[25,27]

The onset of the feature around 1.7 eV corresponds to $2C$-$2H$. We note the series of evenly spaced oscil-

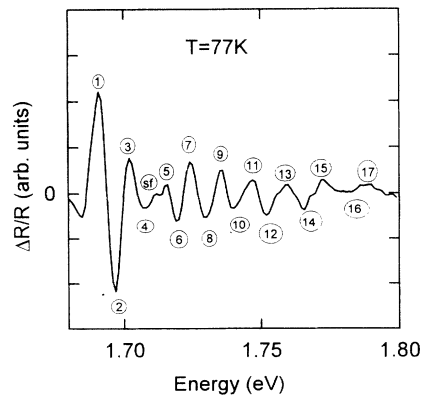

FIG. 2. Experimental photoreflectance spectrum at $T = 77$ K for a quantum-dot array showing the oscillatory features above the $2C$-$2H$ transition in Fig. 1 on an expanded scale.

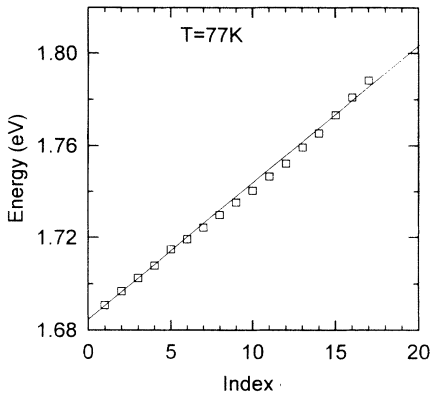

FIG. 3. Plot of the extrema positions above the $2C$-$2H$ transition of Fig. 3 as a function of the extrema index. This straight-line plot supports the model of in-plane harmonic lateral confinement for each quantum dot.

lations extending for about 100 meV. These resonances have been found to be reproducible. Displayed in Fig. 2 is an expanded version of the spectrum in the region of $2C$-$2H$. The various peaks have been labeled with index number $\ell = 1 - 17$. In Fig. 3 is plotted $(E_\ell - E_{2C\text{-}2H})$ vs index ℓ, where E_ℓ is the energy of the ℓth resonance. Note the linear relationship.

There are a number of significant aspects of the spectrum of Fig. 2 such as (a) the spacing between successive resonances (i.e., the slope of Fig. 3), (b) the relative intensities of the various peaks, and (c) the small feature between $\ell = 4$ and $\ell = 5$, labeled "sf". As we shall demonstrate below, our calculations will be able to account for all of these aspects of the PR spectrum. For example, these small features (such as "sf") are related to the depolarization shift which is found to be anisotropic in different directions of the wave vector. In the absence of the Coulomb interaction, some excited states are degenerate due to the square symmetry of the lattice structure and we do not observe these small features in the derivative of the absorption coefficient. However, the Coulomb interaction between electrons depends on the direction of the wave vector which lifts the degeneracy in this system and produces these small features as a result of the splitting of the absorption peaks. The strength of the small features is determined by the optical broadening parameter.

III. OPTICAL ABSORPTION COEFFICIENT FOR QUANTUM-DOT ARRAYS

In this section, we present a model for an array of quantum dots in the x-y plane and a self-consistent field theory for the infrared absorption coefficient. We carry out a detailed calculation of the infrared absorption spectra as a function of the incident photon energy. Here, the many-body depolarization effect is included.

When the electron gas with a positive jellium background is perturbed by an external electric field, the induced density distribution of the electrons will oscillate with a normal mode frequency. The resulting density

fluctuation will introduce an effective dynamic dipole in the system. Since the wavelength of the incident mid-infrared light is much larger than the size of the sample being measured, we assume that the electric field which is propagating along the z direction and polarized in the x-y plane is uniform within the sample. In a quantum dot array of thickness L_z, the coupling of the induced dipole to the external electric field gives rise to energy absorption which is represented by the absorption coefficient we now derive. In our calculations, since we are interested in modeling the dominant $2C$-$2H$ transition features in Fig. 2, we only include excitations from the second electron to the second heavy-hole subbands with envelope functions $\zeta_2^C(z)$, $\zeta_2^{\rm HH}(z)$.

In linear response theory, the induced electron density of frequency ω due to an external electric field $\mathbf{E}_0^{\rm ext}e^{i\omega t}$ is given by

$$\delta\mathcal{N}_{\rm ind}(\mathbf{r},z;\omega) = 2\zeta_2^C(z)\zeta_2^{\rm HH}(z)\sum_{nm}\sum_{n'm'}\psi^*_{n'm'}(\mathbf{r})\,\psi_{nm}(\mathbf{r}) \times\Pi_{NM,N'M'}(\omega)\langle nm|H_1|n'm'\rangle\ , \quad (1)$$

where $\mathbf{r}$ is a 2D vector in the x-y plane,

$$\Pi_{NM,N'M'}(\omega) = \frac{f_0(E_{NM}) - f_0(E_{N'M'})}{\hbar\omega - (E_{N'M'} - E_{NM}) + i\hbar/\tau}\ , \quad (2)$$

$f_0(E)$ is the Fermi distribution function, τ is a phenomenological optical broadening parameter, and the matrix element of the perturbed part of the Hamiltonian consisting of the external and induced potentials due to density fluctuations is

$$\langle nm|H_1|n'm'\rangle = e\mathbf{E}_0^{\rm ext}\cdot\mathbf{r}_{nm;n'm'} + \sum_{\mathbf{q}}v(q)F_{nm;n'm'}(\mathbf{q}) \times\Big[\int_{-\infty}^{\infty}dz''\ e^{-q|z-z''|}\zeta_2^{\rm e}(z'') \times\zeta_2^{\rm HH}(z'')\Big]\delta\mathcal{N}_{\rm ind}(\mathbf{q};\omega)\ , \quad (3)$$

where we have assumed that the wavelength of the incident light is much larger than L_z. In this notation, $v(q) = 2\pi e^2/\epsilon_s q$ where $\epsilon_s = 4\pi\varepsilon_0\epsilon_b$ with ϵ_b denoting the averaged optical dielectric constant of the system. The form factor is defined as $F_{nm;n'm'}(\mathbf{q}) \equiv < nm|e^{-i\mathbf{q}\cdot\mathbf{r}}|n'm' >$, the dipole transition matrix element is $e\mathbf{r}_{nm;n'm'} \equiv \langle nm|e\mathbf{r}|n'm'\rangle$, the envelope functions in the z direction for an electron and a hole are $\zeta_i^C(z)$ and $\zeta_j^{\rm HH}(z)$, respectively, and $\langle\mathbf{r}|nm\rangle \equiv \psi_{nm}(\mathbf{r})$ is the Bloch wave function for electrons or holes within the 2D plane, where $n = (N,k_x)$, $m = (M,k_y)$ are composite indices labeling the eigenstates of the harmonic oscillator potential and the Bloch state wave vectors within the first reducible Brillouin zone. We take the envelope functions for an electron and a hole as $\zeta_i^C(z) = (2\kappa_C^2/\pi)^{1/4}\exp(-\kappa_C^2z^2)H_i(\kappa_C z)$ and $\zeta_i^{\rm HH}(z) = (2\kappa_H^2/\pi)^{1/4}\exp(-\kappa_H^2z^2)H_i(\kappa_C z)$, where $\kappa_C^2 \equiv m_C^*\omega_C/\hbar$ and $\kappa_H^2 \equiv m_H^*\omega_H/\hbar$, with electron effective mass m_C^*, the absolute value of the hole effective mass denoted by m_H^*, and $H_i(x)$ the ith Hermite polynomial. The strengths of the quantum well potentials of the electrons ω_C and holes ω_H are determined from the valence and conduction band offsets,

$$\Delta E_v = \tfrac{1}{2}m_H^*\omega_H^2\left(\frac{L_z}{2}\right)^2\ ,$$

$$\Delta E_c = \tfrac{1}{2}m_C^*\omega_C^2\left(\frac{L_z}{2}\right)^2\ ,$$

where the quantum well is simulated by a truncated parabolic well of width L_z. The eigenfunctions are given by $\psi_{nm}(\mathbf{r}) = \phi_n(x)\phi_m(y)$, where

$$\phi_n(x) = \sum_j e^{ijk_xd_x}\phi_N^{(0)}(x - jd_x)/\sqrt{N_x}\ ,$$

$$\phi_m(y) = \sum_j e^{ijk_yd_y}\phi_M^{(0)}(y - jd_y)/\sqrt{N_y}\ , \quad (4)$$

d_x, N_x and d_y, N_y are the lattice spacings and the number of unit cells in the x and y directions, respectively, and $\phi_N^{(0)}(x), \phi_M^{(0)}(y)$ are the harmonic oscillator eigenfunctions in the x-y plane. For the Bloch wave functions in Eq. (4), the form factor in Eq. (3) is given by $F_{nm;n'm'}(\mathbf{q}) = F_{nn'}(q_x)F_{mm'}(q_y)$ with

$$F_{nn'}(q_x) = \delta_{k_x',k_x+q_x+G_x} \times\int_{-\infty}^{\infty}dx\ e^{-iq_xx}\phi_N^{(0)}(x)\phi_{N'}^{(0)}(x)\ ,$$

$$F_{mm'}(q_y) = \delta_{k_y',k_y+q_y+G_y} \times\int_{-\infty}^{\infty}dy\ e^{-iq_yy}\phi_M^{(0)}(y)\phi_{M'}^{(0)}(y)\ , \quad (5)$$

where G_x, G_y are reciprocal lattice vectors. We have assumed in Eq. (5) that there is no overlap of the wave functions on different quantum dots corresponding to isolated dots in the samples used in the experiment. If θ is the polarization angle which the external electric field makes with the positive x axis and $\hat{\mathbf{e}}_0 = \mathbf{E}_0^{\rm ext}/|\mathbf{E}_0^{\rm ext}|$ is a unit vector in the direction of the external electric field,

$$\mathbf{r}_{nm;n'm'}\cdot\hat{\mathbf{e}}_0 = x_{nm;n'm'}\cos\theta + y_{nm;n'm'}\sin\theta\ , \quad (6)$$

where $x_{nm;n'm'} = X_{nn'}X_{mm'}$ and $y_{nm;n'm'} = Y_{nn'}Y_{mm'}$. Invoking the same assumption as in Eq. (5), we obtain

$$X_{nn'} = \delta_{k_x',k_x+G_x}\int_{-\infty}^{\infty}dx\ \phi_N^{(0)}(x)x\phi_{N'}^{(0)}(x) +i\frac{2d_x}{N_x}\int_{-\infty}^{\infty}dx\ \phi_N^{(0)}(x)\phi_{N'}^{(0)}(x) \times\sum_j j\sin[(k_x' - k_x)jd_x]\ ,$$

$$X_{mm'} = \delta_{k_y',k_y+G_y}\int_{-\infty}^{\infty}dy\ \phi_M^{(0)}(y)\phi_{M'}^{(0)}(y)\ , \quad (7)$$

$$Y_{nn'} = \delta_{k_x',k_x+G_x}\int_{-\infty}^{\infty}dx\ \phi_N^{(0)}(x)\phi_{N'}^{(0)}(x)\ ,$$

$$Y_{mm'} = \delta_{k'_y,k_y+G_y}\int_{-\infty}^{\infty} dy\ \phi_M^{(0)}(y)y\phi_{M'}^{(0)}(y)$$
$$+i\frac{2d_y}{N_y}\int_{-\infty}^{\infty} dy\ \phi_M^{(0)}(y)\phi_{M'}^{(0)}(y)$$
$$\times\sum_j j\sin[(k'_y-k_y)jd_y]\ . \quad (8)$$

The Fourier transform of the induced density fluctuation is

$$\delta\mathcal{N}_{\rm ind}(\mathbf{q};\omega) = \frac{1}{A}\int d\mathbf{r}\ \delta\mathcal{N}_{\rm ind}(\mathbf{r};\omega)\,e^{i\mathbf{q}\cdot\mathbf{r}}\ , \quad (9)$$

where $A = N_xN_yd_xd_y$ denotes the area of the sample. By defining

$$V_{nm;n'm'}(\omega) = \sum_{\mathbf{q}} U(q)F_{nm;n'm'}(\mathbf{q})\delta\mathcal{N}_{\rm ind}(\mathbf{q};\omega)\ , \quad (10)$$

where $U(q) = v(q)I(q)$ with

$$I(q) \equiv \int_{-\infty}^{\infty}dz\int_{-\infty}^{\infty}dz'\ \zeta_2^C(z)\zeta_2^{\rm HH}(z)$$
$$\times e^{-q|z-z'|}\zeta_2^C(z')\zeta_2^{\rm HH}(z')\ , \quad (11)$$

we obtain

$$\left(\frac{V_{ij;i'j'}(\omega)}{e\,|\mathbf{E}_0^{\rm ext}|}\right) = 2\sum_{nm}\sum_{n'm'}\Pi_{NM,N'M'}(\omega)$$
$$\times\left[\mathbf{r}_{nm;n'm'}\cdot\hat{\mathbf{e}}_0+\left(\frac{V_{nm;n'm'}(\omega)}{e\,|\mathbf{E}_0^{\rm ext}|}\right)\right]$$
$$\times\left[\frac{1}{A}\sum_{\mathbf{q}}F^*_{nm;n'm'}(\mathbf{q})F_{ij;i'j'}(\mathbf{q})U(q)\right]\ . \quad (12)$$

Equations (1) and (3) jointly give the polarizability $\alpha_L(\omega)$ of the 2D rectangular array of quantum dots. We have

$$\alpha_{\rm L}(\omega) \equiv \frac{-e}{|\mathbf{E}_0^{\rm ext}|}\frac{1}{L_zA}\int d\mathbf{r}\ \delta\mathcal{N}_{\rm ind}(\mathbf{r};\omega)\,\mathbf{r}\cdot\hat{\mathbf{e}}_0$$
$$= -\frac{2e^2}{L_zA}\sum_{nm}\sum_{n'm'}\left(\mathbf{r}^*_{nm;n'm'}\cdot\hat{\mathbf{e}}_0\right)\Pi_{NM,N'M'}(\omega)$$
$$\times\left[(\mathbf{r}_{nm;n'm'}\cdot\hat{\mathbf{e}}_0)+\left(\frac{V_{nm;n'm'}(\omega)}{e\,|\mathbf{E}_0^{\rm ext}|}\right)\right]\ . \quad (13)$$

Equations (12) and (13) are the two main results of this section. They determine the absorption coefficient of light of frequency ω which is given by

$$\beta_{\rm abs}(\omega) = \frac{\omega}{c\varepsilon_0 n_r(\omega)}\ [\rho_{\rm ph}(\omega)+1]\ {\rm Im}\ \alpha_L(\omega)\ , \quad (14)$$

where $\rho_{\rm ph}(\omega) = 1/\left[e^{\hbar\omega/k_BT}-1\right]$ is the photon distribution function, and the refractive index is given by

$$n_{\rm r}(\omega) = \frac{1}{\sqrt{2}}\left[\epsilon_b+\frac{{\rm Re}\ \alpha_L(\omega)}{\varepsilon_0}+\sqrt{\left(\epsilon_b+\frac{{\rm Re}\,\alpha_L(\omega)}{\varepsilon_0}\right)^2+\left(\frac{{\rm Im}\ \alpha_L(\omega)}{\varepsilon_0}\right)^2}\ \right]^{1/2}\ . \quad (15)$$

In the Appendix, we make use of the results in Eqs. (5)–(8) to express the self-consistent equation for $V_{ij;i'j'}(\omega)/e\,|\mathbf{E}_0^{\rm ext}|$ in matrix form suitable for doing numerical calculations along with the Lorentz ratio in Eq. (13).

Assuming that the frequency of the incident light lies in the interband excitation regime, we include only the transitions between electron and heavy-hole subbands in our numerical calculations. Furthermore, the quantum-dot array is buried in a symmetrical quantum well so that the dominant transitions in this case are $1C$-$1H$ and $2C$-$2H$. The doping electrons occupy the first electron subband. Therefore, the only observed electronic transitions within the quantum dots at low temperatures are between the energy levels superimposed on the second conduction and heavy-hole valence subbands. In our numerical calculations, we only include the transitions superimposed on the interband transition $2C$-$2H$. If the incident light is unpolarized, we must average over the polarization angle θ between 0 and 2π (see the Appendix).

IV. NUMERICAL RESULTS AND EXPERIMENTAL DATA

In this section, we present numerical results for the absorption spectrum of unpolarized incident light in a square array of quantum dots. In principle, our model can be used in quite general cases. However, we do not attempt to make a quantitative comparison with the experimental data since this would involve large-scale computer calculations. Instead, we apply our model to an example with a small number of electrons in each dot. The parameters used in our numerical demonstrations are as follows:

$$L_z = 80\ \text{Å},\ \epsilon_b = 12.0,\ n_{2\rm D} = 0.8\times10^{12}\ {\rm cm}^{-2},$$
$$\Delta E_v = 70\ {\rm meV},\ \Delta E_c = 280\ {\rm meV},\ \hbar/\tau = 0.75\ {\rm meV},$$
$$d_x = d_y = 150\ \text{Å},\ m_C^* = 0.067m_0,\ m_H^* = 0.48m_0,$$
$$E_g = 1.32\ {\rm eV},\ E_2^C = 120\ {\rm meV},\ E_2^{\rm HH} = 24\ {\rm meV}.$$

In this notation, E_g is the intrinsic energy gap of the material, and $E_2^C, E_2^{\rm HH}$ are the band edges for the second electron and second heavy-hole subbands. We use parabolic confining potentials of frequency Ω_C and Ω_H, respectively, for the electrons and holes. In our calculations, we have included three degenerate in-plane electron energy levels. The in-plane quantum numbers are

$$(N',M') = (1,0),\ (0,1),\ (0,3),$$
$$(1,2),\ (2,1),\ (3,0),$$

whose energies are given by Eq. (A12).

In Figs. 4(a), 5(a), and 6(a), the absorption coefficient [in units of $\alpha_0 = e^2/(\hbar c \varepsilon_0 a_0^*)$, where $a_0^* = \epsilon_s \hbar^2/(m_C^* e^2)$] is plotted as a function of the photon energy $\hbar\omega$ at temperature $T = 77$ K for three pairs of values of Ω_C and Ω_H. There are two peaks which correspond to the transitions between the discrete energy levels within a quantum dot. The many-body depolarization shift depends on the form factors and lifts the degeneracy to some extent.

In Figs. 4(b), 5(b), and 6(b), the derivatives of the absorption coefficient in Figs. 4(a), 5(a) and 6(a) are plotted as a function of $\hbar\omega$. As in Fig. 2, we have labeled the various peaks with index number ℓ. The absorption peaks arising from the interband transitions produce the sign changes in the derivative of the absorption coefficient. The zero in the derivative spectrum corresponds to the peak or valley positions in the absorption coefficient. There are four peaks in the spectrum. The features in the absorption spectrum are significantly amplified in its derivative, thereby providing a way of determining the confining environment from the values of Ω_C and Ω_H by fitting the line shape of the thermally broadened absorption spectrum.

The results in Figs. 4(b), 5(b), and 6(b) show that the details of the derivative spectra, *i.e.*, spacing and relative intensities of the peaks and valleys as well as small features, depend sensitively on the values that we choose for the parameters Ω_C and Ω_H. For example, there is clearly a reduction in the spacing of the extrema, i.e. the slope of energy as a function of the index number ℓ (such as Fig. 3) as Ω_C and Ω_H are decreased. The relative intensities of the peaks/valleys also are controlled by these quantities. In Fig. 4(b), structure $\ell = 5/\ell = 6$ has about the same amplitude as the leading feature $\ell = 1/\ell = 2$, while in Fig. 6(b) the relative amplitudes are more similar

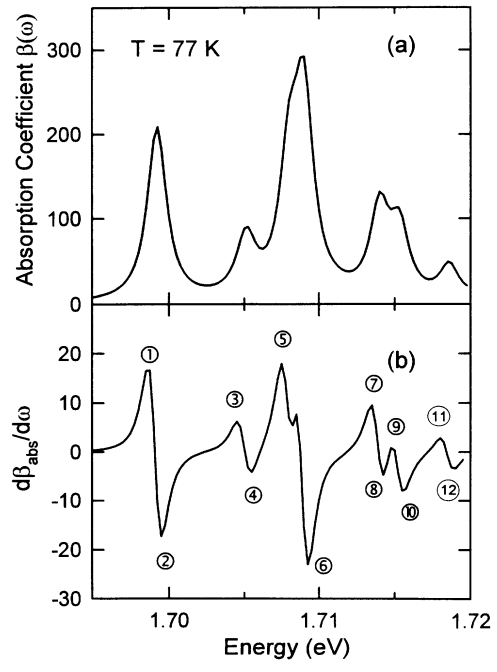

FIG. 4. (a) Calculated absorption coefficient at $T = 77$ K as a function of the photon energy. This calculation is based on the full many-body theory for unpolarized incident light with $\hbar\Omega_C = 9$ meV and $\hbar\Omega_H = 6$ meV. (b) Calculated derivative of the absorption coefficient as a function of the photon energy.

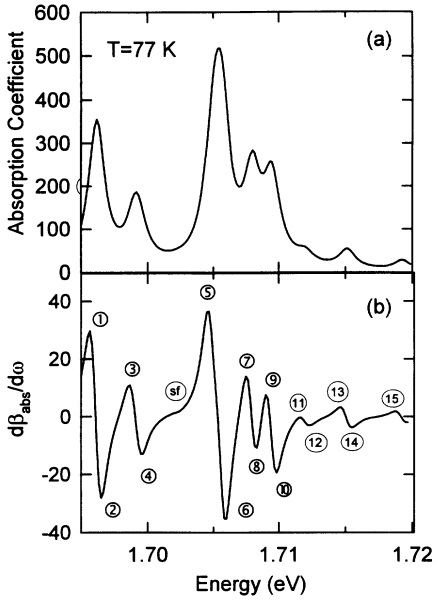

FIG. 5. (a) Calculated absorption coefficient at $T = 77$ K with $\hbar\Omega_C = 9$ meV and $\hbar\Omega_H = 3$ meV. (b) Calculated derivative of the absorption coefficient as a function of the photon energy.

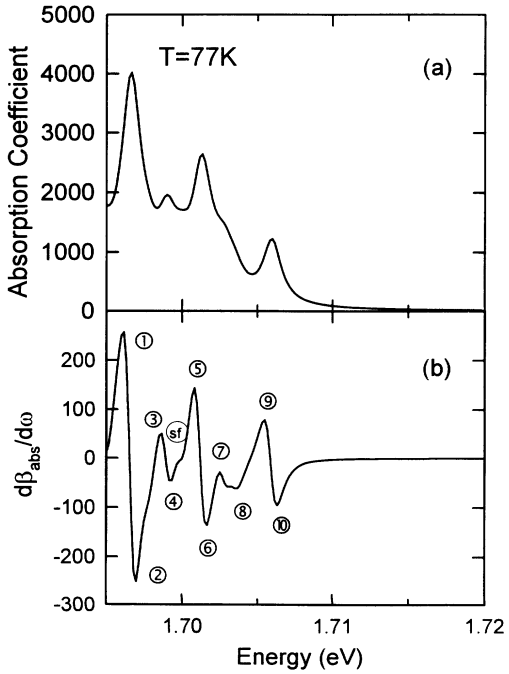

FIG. 6. (a) Calculated absorption coefficient at $T = 77$ K with $\hbar\Omega_C = 4.5$ meV and $\hbar\Omega_H = 3$ meV. (b) Calculated derivative of the absorption coefficient as a function of the photon energy.

to the experimental data of Fig. 2. In Fig. 4(b) there is no "sf" between features 4 and 5 while in Figs. 5(b) and 6(b) such a structure is clearly visible. Therefore, by the appropriate choice of Ω_C and Ω_H, it would be possible to reproduce the details of Fig. 2. This means that the effects due to the Coulomb interaction between electrons are related to the degree of confinement within a quantum dot. Our calculations also show that the derivative spectrum depends on the temperature.

V. CONCLUDING REMARKS AND SUMMARY

In conclusion, we have used harmonic potentials to simulate lateral confinement of quantum dots. We have derived a self-consistent field theory for the infrared absorption of polarized or unpolarized incident light in this system. The derivative spectrum depends on the values of Ω_C and Ω_H, thereby providing a means of simulating the confining environment due to the surface charge on the quantum dots, by comparing with the photoreflectance spectrum. Many of the observed features in the experiments reported here are reproduced in our theory. The features in the absorption spectrum are significantly amplified. The thermal broadening of the peaks sensitively depends on the electron density and the temperature. Based on the known temperature in the experiment, it gives us a convenient way of determining the number of electrons in each dot by fitting the thermally broadened line shape.

ACKNOWLEDGMENTS

The authors G.G. and D.H. acknowledge the support in part from the City University of New York PSC-CUNY Grant No. 662505 and the Office of Naval Research under Contract No. N00014-93-1-0576 while the authors H.Q. and F.H.P. wish to acknowledge NSF Grant No. DMR-9120363, PSC-CUNY Grant No. 664239, and NATO travel Grant No. 5-2-05/RG-920115. The authors P.D.W., C.M.S.T., and M.C.H. received support from the U.K. Science and Engineering Research Council Grant No. GR/H44714. They also acknowledge the NATO travel grant. We benefited from several critical comments by Joseph Birman and Norman Horing.

APPENDIX

In this Appendix, we simplify the results in Eqs. (12) and (13) by making use of the results in Eqs. (5)–(8). In a straightforward way, we have shown that as $N_x \to \infty$

$$\alpha_L(\omega) = -e^2 N_e \sum_{NM} \sum_{N'M'} (\mathbf{r}_{NM;N'M'} \cdot \hat{\mathbf{e}}_0)\, \Pi_{NM,N'M'}(\omega) \times \left[(\mathbf{r}_{NM;N'M'} \cdot \hat{\mathbf{e}}_0) + \left(\frac{V_{NM;N'M'}(\omega)}{e\,|\mathbf{E}_0^{\rm ext}|} \right) \right] , \tag{A1}$$

where N_e is the total number of electrons within the 2D plane and

$$\mathbf{r}_{NM;N'M'} \cdot \hat{\mathbf{e}}_0 = X_{NN'} X_{MM'} \cos\theta + Y_{NN'} Y_{MM'} \sin\theta . \tag{A2}$$

Here,

$$X_{NN'} = \int_{-\infty}^{\infty} dx\ \phi_N^{(0)}(x) x \phi_{N'}^{(0)}(x) ,$$

$$X_{MM'} = \int_{-\infty}^{\infty} dy\ \phi_M^{(0)}(y) \phi_{M'}^{(0)}(y) . \tag{A3}$$

$$Y_{NN'} = \int_{-\infty}^{\infty} dx\ \phi_N^{(0)}(x) \phi_{N'}^{(0)}(x) ,$$

$$Y_{MM'} = \int_{-\infty}^{\infty} dy\ \phi_M^{(0)}(y) y \phi_{M'}^{(0)}(y) . \tag{A4}$$

Also,

$$V_{NM;N'M'}(\omega) \equiv \sum_{\mathbf{G}_{\ell\ell'}} U(\mathbf{G}_{\ell\ell'}) F_{NM;N'M'}(\mathbf{G}_{\ell\ell'}) \times \delta\mathcal{N}_{\rm ind}(\mathbf{G}_{\ell\ell'};\omega) , \tag{A5}$$

where $\mathbf{G}_{\ell\ell'} = (2\pi\ell/d_x, 2\pi\ell'/d_y)$ with ℓ, ℓ' being integers is a reciprocal lattice vector and

$$F_{NM;N'M'}(\mathbf{G}_{\ell\ell'}) = f_{NN'}(2\pi\ell/d_x) f_{MM'}(2\pi\ell'/d_y) . \tag{A6}$$

In this notation,

$$f_{NN'}(2\pi\ell/d_x) = \int_{-\infty}^{\infty} dx\ e^{-i2\pi\ell x/d_x} \phi_N^{(0)}(x) \phi_{N'}^{(0)}(x) ,$$

$$f_{MM'}(2\pi\ell'/d_y) = \int_{-\infty}^{\infty} dy\ e^{-i2\pi\ell' y/d_y} \phi_M^{(0)}(y) \phi_{M'}^{(0)}(y) . \tag{A7}$$

The matrix equation determining $V_{NM;N'M'}(\omega)$ is

$$\sum_{NM} \sum_{N'M'} \left\{ \delta_{NI}\delta_{MJ}\delta_{N'I'}\delta_{M'J'} - n_{\rm 2D} \gamma_{IJ,I'J'}^{NM,N'M'} \chi_{NM,N'M'}(\omega) \right\} \left(\frac{V_{NM;N'M'}(\omega)}{e\,|\mathbf{E}_0^{\rm ext}|} \right) = n_{\rm 2D} \sum_{NM} \sum_{N'M'} \gamma_{IJ,I'J'}^{NM,N'M'} \chi_{NM,N'M'}(\omega) (\mathbf{r}_{NM;N'M'} \cdot \hat{\mathbf{e}}_0) , \tag{A8}$$

where

$$\chi_{NM,N'M'}(\omega) = [f_0(E_{NM}) - f_0(E_{N'M'})]|_{E_{NM} < E_{N'M'}} \times \left[\frac{1}{\hbar\omega - (E_{N'M'} - E_{NM}) + i\hbar/\tau} - \frac{1}{\hbar\omega + (E_{N'M'} - E_{NM}) + i\hbar/\tau} \right] , \tag{A9}$$

n_{2D} is the areal electron density and

$$\gamma_{IJ,I'J'}^{NM,N'M'} \equiv \sum_{\mathbf{G}_{\ell\ell'}} F_{NM;N'M'}^{*}(\mathbf{G}_{\ell\ell'}) F_{IJ;I'J'}(\mathbf{G}_{\ell\ell'}) U(G_{\ell\ell'}) \ . \tag{A10}$$

We replace $\mathbf{r}_{NM;N'M'} \cdot \hat{\mathbf{e}}_0$ in (A2) by $[(X_{NN'}X_{MM'})^2 + (Y_{NN'}Y_{MM'})^2]^{1/2}/\sqrt{2}$ when we average over the angle θ. The only nonzero contributions to (A8) come from the terms with $N+N'$ even and $M+M'$ odd and vice versa.

We use parabolic confining potentials for the electrons and holes and denote the frequency of the harmonic oscillator potential by Ω_C and Ω_H, respectively. For this model, the heavy-hole energy is

$$E_{NM} = -(N+M+1)\,\hbar\Omega_H - (E_2^{\mathrm{HH}} + E_g) \ , \tag{A11}$$

and the electron energy is

$$E_{N'M'} = (N'+M'+1)\,\hbar\Omega_C + E_2^C \ , \tag{A12}$$

where $N, M, N', M' = 0, 1, 2, \ldots$. In this notation, E_g is the intrinsic energy gap of the material, and E_2^C, E_2^{HH} are the band edges for the second electron and second heavy-hole subbands with envelope functions $\zeta_2^C(z), \zeta_2^{\mathrm{HH}}(z)$.

Since the peak positions of the PR spectrum are equally spaced, we conclude that only excitations from the topmost heavy-hole level ($N+M=0$) are effectively excited in the experiment. This might be due to the considerable overlap of the broadened heavy-hole levels when the separation between these energy levels is small. Consequently, we get $E_{N'M'} - E_{00} = (E_2^C + E_2^{\mathrm{HH}} + E_g + \hbar\Omega_H) + (N'+M'+1)\hbar\Omega_C$ where $N'+M'$ is an odd integer. From the known values of E_2^C, E_2^{HH}, E_g, and the first peak position as well as the peak separation, we can easily determine the values of Ω_C, and Ω_H, respectively.

* Also at The Graduate School and University Center of the City University of New York, New York, NY 10036.
† Present address: Department of Electrical and Computer Engineering, Wayne State University, Detroit, MI 48202.

[1] D. Heitmann and J. P. Kotthaus, Phys. Today **46** (6), 56 (1993); D. Heitmann, T. Demel, P. Grambow, M. Kohl, and K. Ploog, in *Proceedings of the International Conference on the Physics of Semiconductors, Thessaloniki, 1990,* edited by E. M. Anastassakis and J. D. Joannopoulos (World Scientific, Singapore, 1990), p. 13.
[2] C. Weisbuch and B. Vinter, *Quantum Semiconductor Structures: Fundamentals and Applications* (Academic, New York, 1991).
[3] B. Kapon, D. M. Huang, and R. Bhat, Phys. Rev. Lett. **63**, 430 (1989).
[4] H. Benistry, C. M. Sotomayor Torres, and C. Weisbuch, Phys. Rev. B **42**, 8947 (1991).
[5] H. Benistry, in *Phonons in Semiconductor Nanostructures*, edited by J.-P. LeBurton, J. Pascual, and C. M. Sotomayor Torres (Kluwer, Dordrecht, 1993), p. 447.
[6] P. D. Wang and C. M. Sotomayor Torres, J. Appl. Phys. **74**, 5047 (1993).
[7] K. F. Berggren *et al.*, Phys. Rev. Lett. **57**, 1769 (1986).
[8] M. A. Reed, Sci. Am. **268** (1), 118 (1993).
[9] D. Huang and P. R. Antoniewicz, Phys. Rev. B **43**, 2169 (1991).
[10] D. A. Broido, K. Kempa, and P. Bakshi, Phys. Rev. B **42**, 11 400 (1990).
[11] P. Bakshi, D. A. Broido, and K. Kempa, Phys. Rev. B **42**, 7416 (1990).
[12] T. Demel, D. Heitmann, P. Grambow, and K. Ploog, Phys. Rev. Lett. **64**, 788 (1990).
[13] T. P. Smith, K. Y. Lee, C. M. Knoedler, J. M. Hong, and D. P. Kern, Phys. Rev. B **38**, 2172 (1988).
[14] C. Zhang, G. Gumbs, and D. Huang, Phys. Rev. B **44**, 10 744 (1991).
[15] U. Meirav, M. A. Kastner, and S. J. Wind, Phys. Rev. Lett. **65**, 771 (1990); M. A. Kastner, Phys. Today **46** (1), 24 (1993); Rev. Mod. Phys. **64**, 849 (1992).
[16] Y. Meir, N. S. Wingreen, and P. A. Lee, Phys. Rev. Lett. **66**, 3048 (1991).
[17] C. M. Sotomayor Torres, A. P. Smart, M. A. Foad, and C. D. W. Wilkinson, in *Festkörperprobleme*, edited by U. Rössler, *Advances in Solid State Physics* Vol. 32 (Viewig, Braunschweig/Weisbaden, 1992), p. 265; R. Cheung, S. Thoms, M. Watt, M. A. Foad, C. M. Sotomayor Torres, C. D. W. Wilkinson, U. J. Cox, R. A. Cowley, C. Dunscombe, and R. H. Williams, Semicond. Sci Technol. **7**, 1189 (1992).
[18] F. H. Pollak and H. Shen, Mater. Sci. Eng. **R10**, 275 (1993).
[19] O. J. Glembocki and B. V. Shanabrook, in *Semiconductors and Semimetals*, edited by D. G. Seiler and C. L. Littler (Academic, New York, 1992), Vol. 36, p. 222.
[20] Y.-S. Tang, C. D. W. Wilkinson, C. M. Sotomayor Torres, D. W. Smith, T. E. Whall, and E. H. C. Parker, Superlatt. Microstruct. **12**, 535 (1992); Solid State Commun. **85**, 199 (1993).
[21] H. Qiang, F. H. Pollak, Y.-S. Tang, P. D. Wang, and C. M. Sotomayor Torres, Appl. Phys. Lett. **64**, 2830 (1994); in *Quantum Well and Superlattice Physics V*, edited by G. H. Döhler and E. S. Koteles, SPIE Proc. Vol. 2139 (SPIE Bellingham, WA, 1994), p. 234.
[22] G. Mei, S. Carpenter, L. E. Felton, and P. D. Persans, J. Opt. Soc. Am. B **9**, 1394 (1992); P. D. Persans, M. Silvestri, G. Mei, E. Lu, H. Yuselici, and J. Schroeder, Braz. J. Phys. **23**, 144 (1993); F. Hache, D. Ricard, and C. Flytzanis, Appl. Phys. Lett. **55**, 1504 (1989).
[23] P. D. Wang, C. M. Sotomayor Torres, M. C. Holland, H. Qiang, F. H. Pollak, and G. Gumbs, in *Diagnostic Techniques for Semiconductor Materials Processing*, edited by O. J. Glembocki, F. H. Pollak, S. W. Pang, G. Larrabee, and G. M. Crean, MRS Symposia Proceedings No. 324 (Materials Research Society, Pittsburgh, 1994), p. 187.
[24] G. Gumbs, D. Huang, Y. Yin, H. Qiang, D. Yan, F. H. Paollak, and T. F. Noble, Phys. Rev. B **48**, 18 328 (1993).
[25] Y. Yin, H. Qiang, F. H. Pollak, D. C. Streit and M. Wojtowicz, Appl. Phys. Lett. **61**, 1579 (1992); in *Quantum Well and Superlattice Physics IV*, edited by G. H. Döhler and E. Koteles, SPIE Proc. Vol. 1675 (SPIE, Bellingham, WA, 1992), p. 498.
[26] A. Dimoulas, K. Zekentes, M. Androulidaki, N. Kornelios, C. Michelakis, and Z. Hatzopoulos, Appl. Phys. Lett. **63**, 1417 (1993).
[27] Y. Yin, H. Qiang, D. Yan, F. H. Pollak, and T. F. Noble, Semicond. Sci. Technol. **8**, 1599 (1993).